

Circularly Polarized Light Source from Self-Assembled Hybrid Nanoarchitecture

Xiongbin Wang, Qiushi Wang, Xuanyu Zhang, Jun Miao, Jiaji Cheng, Tingchao He,*
Yiwen Li,* Zikang Tang,* and Rui Chen*

Circularly polarized luminescent inorganics arouses attentions due to scalable preparation and versatile chiral optoelectronic applications. Here, strong circularly polarized luminescence (CPL) activity has been developed from self-assembled cellulose nanocrystals decorated with blue emitting silicon quantum dots (QDs). The electrostatic attraction promotes the successful incorporation of QDs into chiral template matrix to form homogeneous hybrid nanoarchitecture films. It is found that their circular dichroism behaviors are closely related to the photonic band gap (PBG) while the CPL behaviors are determined by the QDs and PBG simultaneously. Furthermore, the as-prepared chiral composite thin films have been employed as an efficient circularly polarized light source for preparing enantioselective polymer, which can induce chirality and photopolymerization simultaneously. Such strong CPL activity in nanoarchitecture films is highly promising for future inorganic optoelectronics.

1. Introduction

Circularly polarized luminescence (CPL) is particularly important for its promising potentials in circularly polarized light sources,^[1] enantioselective catalysis,^[2,3] spintronics,^[4–6]

chirality-based light emitting diodes (LEDs),^[7,8] and so forth.^[9,10] Extensive efforts have been applied to a broad range of organic luminophores up till now.^[11] However, only a few CPL-active inorganic nanomaterials have been designed recently due to the complexity of fine controlled chiroptical responses and insufficient theoretical background explaining the origin of chirality.^[12,13] Various approaches have been developed to realize CPL from inorganic nanomaterials. For instance, nanocrystals could exhibit CPL behaviors through the π conjugated interaction between chiral capping ligand and achiral cores.^[12,14] It is also hypothesized that chiral environment could confer CPL on quantum dots (QDs), which has been

evidenced by CdS QDs encapsulated in chiral apoferritin.^[15] However, these approaches usually need tedious synthesis procedures, and the induced CPL signal is usually very low with the dissymmetry factor only $\approx 10^{-3}$ – 10^{-4} .^[12–16] Moreover, it is known that most metal-based nanomaterials are toxic and have the disadvantage of high manufacturing cost, which limit their widespread applications. Under this circumstance, it is urgent to develop environmentally friendly and CPL nanomaterials with high strength and capacity for scalable preparations.

Silicon-based nanoparticles have gained extensive attentions owing to their desirable properties such as being comprised of earth-abundant elements, favorable biocompatibility, and excellent photostability.^[17–19] Fluorescent silicon QDs (Si QDs) have been recognized as a promising material sharing remarkable optical and electronic properties of traditional metal-based semiconductor QDs. In the past decades, considerable efforts have been devoted to investigate their synthetic strategies and practical applications. A variety of green and simple synthetic methods have been developed for preparing this promising material.^[17,20–22] Besides, the excellent water stability, high fluorescence, and low toxicity make them suitable for applications in plenty of fields such as bioimaging, photocatalysis, and sensing.^[23–25] Based on these outstanding properties, Si QDs is undoubtedly a prominent candidate for the implementation of CPL. To the best of our knowledge, conferring CPL on Si QDs has not been reported to date.

Cellulose nanocrystals (CNCs) are renewable and biocompatible nanomaterials which could be easily obtained from bulk cellulose by acid-hydrolysis. After treating with sulfuric acid, CNCs could exhibit excellent water dispersibility due to negative charge from the enriched sulfonate groups on the surfaces.^[26,27]


X. Wang, Z. Tang
The Institute of Applied Physics and Materials Engineering
University of Macau
Avenida da Universidade, Taipa, Macau 999078, P. R. China
E-mail: zktang@um.edu.mo

X. Wang, X. Zhang, R. Chen
Department of Electrical and Electronic Engineering
Southern University of Science and Technology
Shenzhen, Guangdong 518055, P. R. China
E-mail: chenr@sustech.edu.cn

Q. Wang, J. Cheng, Y. Li
School of Materials Science and Engineering
Hubei University
Wuhan, Hubei 430062, P. R. China
E-mail: yiwenli@hubu.edu.cn

J. Miao
Department of Chemistry
Southern University of Science and Technology
Shenzhen, Guangdong 518055, P. R. China

T. He
College of Physics and Optoelectronic Engineering
Shenzhen University
Shenzhen, Guangdong 518060, P. R. China
E-mail: tche@szu.edu.cn

 The ORCID identification number(s) for the author(s) of this article can be found under <https://doi.org/10.1002/adom.202200761>.

DOI: 10.1002/adom.202200761

Besides, the rod-like CNCs with concentration above their critical value could be self-assembled into left-handed chiral nematic structures during the solvent evaporation process.^[28,29] Thanks to this advantage, CNCs is an ideal nanomaterial to construct functional CPL-active platform. Herein, chiral nematic structures with helical assembly of Si QDs are fabricated based on CNCs template. The as-prepared chiral nematic nanoarchitectures exhibit induced chiroptical response in CPL measurements with significant anisotropic factors up to -0.25 . The CPL intensity can be manipulated through the interaction between the emission from Si QDs and the photonic band gap (PBG) of the chiral nematic structure. Finally, CPL emissive films have been prepared and served as circularly polarized light sources for enantioselective polymerization of 10,12-Tricosadiynoic acid (DA) molecules with photoinduced chirality. These findings would provide new insights for micro- and nanomanufacturing such as polarization-tailored nano/micro-patterning, chiroptical information encryption, polarized luminescence, and detection.

2. Results and Discussion

The schematic diagram for the preparation of blue emitting Si QDs and CNCs based chiral composite film is shown in **Figure 1**. Si QDs are synthesized facily according to previous literature.^[24,30] Simply, glucose served as reductant is mixed with 3-aminopropyltriethoxysilane (3-APTES) for aqueous Si QDs preparation at room temperature. Then, the as-prepared Si QDs are transferred into CNCs solution. The positively charged Si QDs could be bound to the rod-like CNCs through electrostatic interaction where the surface of CNCs carries abundant and negatively charged sulfate ester groups. The mixed suspension could spontaneously assemble into left-handed helical

structure during the evaporation-induced self-assembly (EISA) process when the concentration of CNCs above the threshold.^[31] It is found that the self-assembly film emits right-handed CPL under UV lamp illumination. Detailed optical characterizations will be discussed later.

Transmission electron microscopy (TEM) is used to characterize the morphology of the as-prepared Si QDs. It can be seen from **Figure 2a** that the as-prepared nanoparticles display spherical shape with excellent dispersibility which confirms the successful synthesis of Si QDs. The Si QDs possess an average diameter of 3.9 ± 0.1 nm, which is estimated from the size distribution histogram (Figure S1, Supporting Information). The surface functional groups of the as-prepared Si QDs are determined by Fourier Transform infrared (FTIR) spectrum. As shown in Figure 2b, the spectrum exhibits a broad absorption band centered at 3312 cm^{-1} resulting from the combination of stretching vibrations of O–H and N–H. The absorption bands at 2931 and 2879 cm^{-1} are derived to be the C–H and C–H₂ stretching vibrations, respectively. The peak at 1641 cm^{-1} could be regarded as the C=O stretching vibration of carboxylic group. This carboxylic group comes from the oxidation of the ketone, where glucose is used as reducing agent. While the bands at 1560 and 777 cm^{-1} are corresponding to the bending and wagging vibrations of N–H, respectively. The presence of N–H bond indicates that the amine group does not react with ketene in glucose to form Schiff base structure, but is exposed on the surface of the as prepared Si QDs. The peak at 1445 cm^{-1} is due to the bending vibration of C–H, and the peak at 1405 cm^{-1} is attributed to C–O–H bending vibration. The C–N stretching vibration is reflected in 1349 cm^{-1} . The peaks at 1197 and 1010 cm^{-1} are related to Si–O–C band and Si–O–Si stretching vibrations, respectively. The C–O–C bond stretching is centered at 1078 cm^{-1} . The band at 911 cm^{-1} could be ascribed to the Si–O stretching of Si–O–H, and the peak at 869 cm^{-1} is

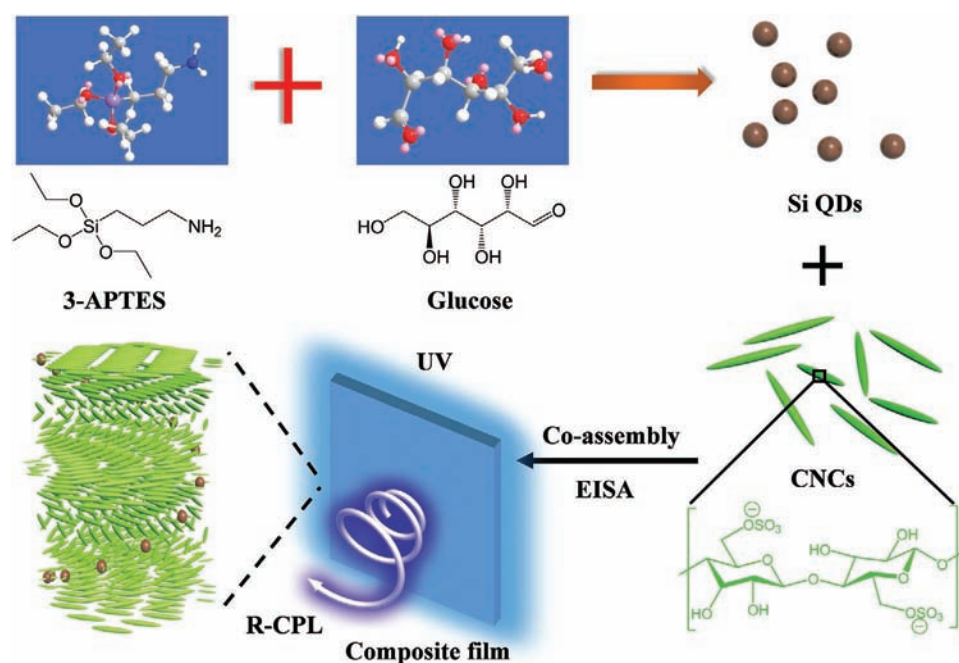


Figure 1. Illustration of the synthesis of Si QDs and the evaporation-induced cooperative assembly of CNCs-Si QDs with tunable PBG and R-CPL.

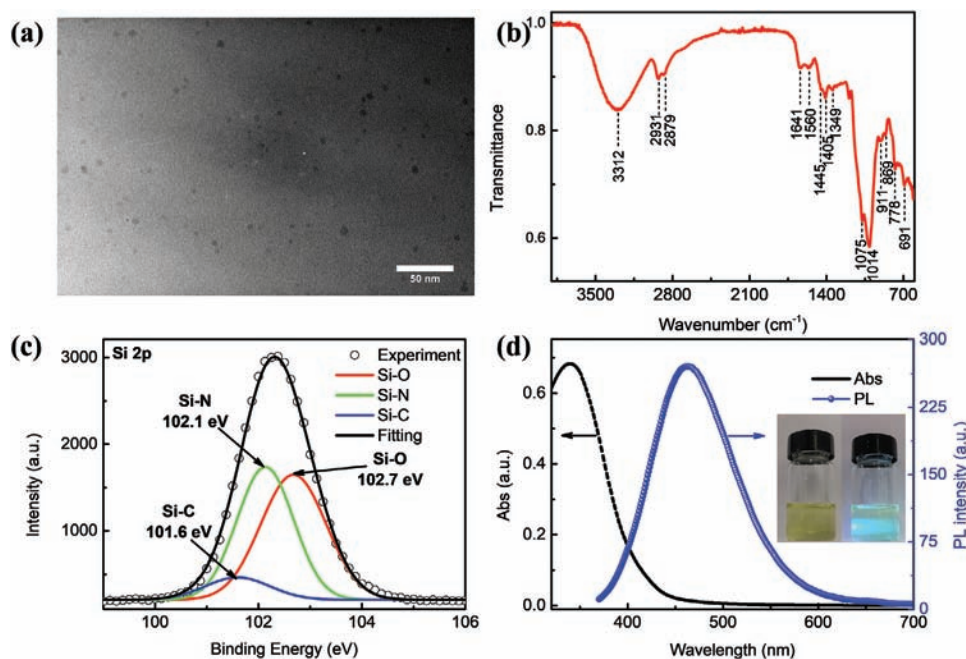


Figure 2. Si QDs characterizations. a) Representative TEM image of the as-prepared Si QDs. b) FTIR spectrum of Si QDs. c) High resolution XPS spectrum of Si 2p orbital. d) Absorption and emission spectra of Si QDs. The inset shows the solution of Si QDs under natural light and a hand-held UV lamp.

due to Si–N stretching vibration. The band at 691 cm^{-1} is owing to the secondary amine vibration.

X-ray photoelectron spectroscopy (XPS) measurement is conducted to further determine the surface composition of the as-prepared Si QDs. As shown in Figure S2a, Supporting Information, the full range XPS data exhibits five major peaks located at 530.1, 398.2, 283.2, 151.3, and 100.5 eV, which correspond to O 1s, N 1s, C 1s, Si 2s, and Si 2p orbitals, respectively. Three peaks of Si 2p are located at 101.6 (Si–C), 102.1 (Si–N), and 102.7 eV (Si–O), which confirm the attached nitrogen and oxygen contained functional groups on the surface of Si QDs (Figure 2c).^[32] Six peaks appear in the C 1s spectrum (Figure S2c, Supporting Information). Two peaks with binding energies of 282.8 and 283.4 eV could be assigned to C–Si. The remaining four peaks at 283.4, 285.5, 286.3, and 287.6 eV belong to C–C/C=C, C–N, C–OH/C–O–C, and C=O, respectively.^[33] Three peaks located at 398.5, 399.7, and 400.7 eV could be attributed to N–Si, C–N–C, and N–(C)₃ (Figure S2d, Supporting Information).^[17] There are three peaks in the spectrum of O 1s. The two peaks located at 530.6 and 532 eV could be ascribed to O–Si, while the peak that appeared at 532.5 eV belongs to O–C (Figure S2b, Supporting Information).^[17] According to these results, it can be concluded that there are plenty of hydrophilic functional groups on the surface of the as-prepared Si QDs which contribute to the superior water solubility.

The as-prepared Si QDs solution exhibits light brown color and acquires intensive blue light emission under UV light irradiation, which can be clearly seen in the inset of Figure 2d. The as-prepared Si QDs show a continuous broad absorption in the range of 300–500 nm with a distinct shoulder at 342 nm, which is consistent with previous reports.^[24,34] A signature symmetrical emission located at 464 nm has been observed under the

excitation of 350 nm. It has been reported that surface defects would dramatically increase when the size of Si QDs is smaller than their Bohr radius of $\approx 4.2\text{ nm}$.^[35] It is known from previous reports that surface defects such as dangling bonds on the surface of Si QDs are responsible to their emission. Hence, since the size of the as-prepared Si QDs is smaller than the Bohr excitonic radius of Si, the observed emission could be ascribed to the defect states on the surface. Apart from this, the Si QDs exhibit red shifted emission accompanying the increase of excitation wavelength. As shown in Figure S3, Supporting Information, the emission shifts from 460 to 471 nm when the excitation wavelength changes from 320 to 380 nm. This slight red shift could be related to the surface functional groups, similar to previous reports,^[36,37] and again confirms that the defects states are responsible for the emission of Si QDs.^[24,38]

The hybrid nanoarchitecture films of Si QDs -CNCs are prepared according to the EISA mechanism at room temperature with various Si QDs concentrations as summarized in Table S1, Supporting Information (a detailed description can be found in Experimental Section). For simplicity, the fabricated films with different Si QDs concentrations from high to low are denoted as S1, S2, S3, and S4 accordingly. As shown in Figure 3a, CNCs prepared from sulfuric acid hydrolysis have spindle-like morphology with an average length from 150 to 200 nm and diameter from 15 to 20 nm respectively, which can be verified from TEM characterizations. After mixing Si QDs with CNCs solutions, there is no flocculation that can be observed. Besides, under UV lamp irradiation, the mixed solution exhibits enhanced emission with the increase of Si QDs concentration. These findings indicate that the introduction of Si QDs in CNCs could form a homogenous solution without quenching the emission of QDs (Figure S4, Supporting Information). To

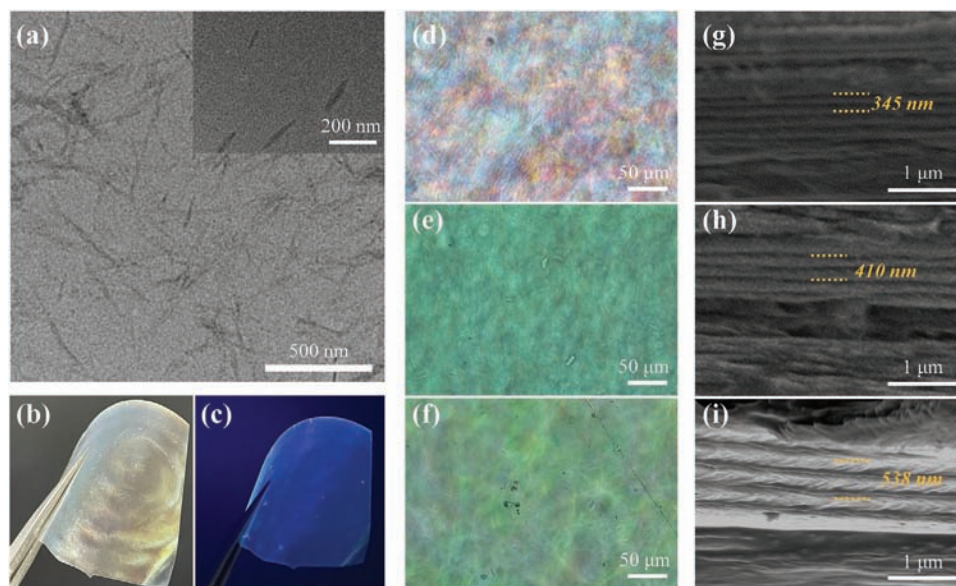


Figure 3. Characterizations of photonic films. a) TEM images of CNCs. Photographs of S2 under b) natural light and c) UV lamp irradiation, respectively. POM images taken with crossed polarizers of the photonic films: d) S1, e) S2, and f) S3. Cross-sectional SEM images of the photonics films: g) S1, h) S2, and i) S3.

investigate the interaction between Si QDs and CNCs, zeta potential measurement is carried out and the results are summarized in Table S2, Supporting Information. The positive charge of Si QDs could be attributed to the exposed amine ends on the surface of the QDs, which is consistent with the results of FTIR. The opposite charges between nanoparticles and the matrix can assist Si QDs to attach on the surface of CNCs' nanorods through electrostatic attraction. Besides, the mixed solutions remain clear even after one month. Although the positively charged Si QDs could reduce the electrostatic repulsion with CNCs, the repulsion is still strong enough to avoid aggregation, which is consistent with the measured zeta potentials data.

As shown in Figure 3b,c, the as-prepared film (S2) is iridescent under natural light corresponding to the 1D photonic crystal structures. Furthermore, S2 exhibits homogeneous and blue emission under UV light, proving that the emission of Si QDs is retained after the EISA process. The as-prepared films are further analyzed by polarized optical microscopy (POM). It could be seen that plenty of fingerprint textures could be observed from the POM images, which confirm the formation of the chiral nematic phase of the composited films.^[39] A helical pitch that is defined as the distance where the CNC nanorods undergo a 360° twist is a key parameter, which determines the property of chiral nematic structures. The distance between two adjacent finger textures observed in POM could be regarded as half of the helical pitch in the structures. The color change in birefringence from blue to light green for S1, S2, and S3 is observed resulting from the increase of helical pitches with the decrease of the Si QDs concentration. It could be understood that electrostatic repulsion between different CNCs is decreased by loading more positively charged Si QDs, which is again confirmed by the measured zeta potentials. Cross-sectional scanning electron microscopy (SEM) measurements

of the fabricated films are shown in Figure 3d–f. The SEM images exhibit periodical layer structure with uniform helical pitches. From the SEM images, the helical pitches are estimated to be 345, 410, and 538 nm for S1, S2, and S3, which is corresponding to the red-shift of color change in birefringence observed in POM images (Figure 3g–i).

Manipulating the reflection and transmission of light is one of the most intriguing characteristics for photonic crystals. For 1D photonic crystal, the wavelength of selective reflection follows Bragg equation, which is expressed as:

$$\lambda_{\max} = n_{\text{avg}} P \sin(\theta) \quad (1)$$

where n_{avg} is the average refractive index of the hybrid film, P is the as-mentioned helical pitch, and θ is the angle between the surface of photonic film and incident light. **Figure 4a** shows the transmission spectrum of the as-prepared photonic crystal films. Two well-resolved peaks could be observed in the transmittance spectrum. The peak located at around 350 nm is originated from the absorption of Si QDs. The very broad band at longer wavelength is corresponded to the selective reflection of the photonic crystal structures. More precisely, the center wavelength of the PBGs is blue-shifted from 540 (S4) to 425 nm (S1) with increasing concentration of Si QDs, which indicates that the decrease of helical pitch is consistent with the SEM characterizations. Besides, the absorption of Si QDs exhibits an increasing tendency with the increase of concentration. The slight red-shift of the absorption might be attributed to aggregation of the QDs during the EISA process.^[40] CD measurement is carried out to investigate the chiral behavior of the as-prepared films. It is known that many artifacts would contribute to the recorded signal.^[26,41] For oriented solid films, linear dichroism (LD) and linear birefringence (LB) are the major artifacts for the electronic recorded CD signal. Nevertheless,

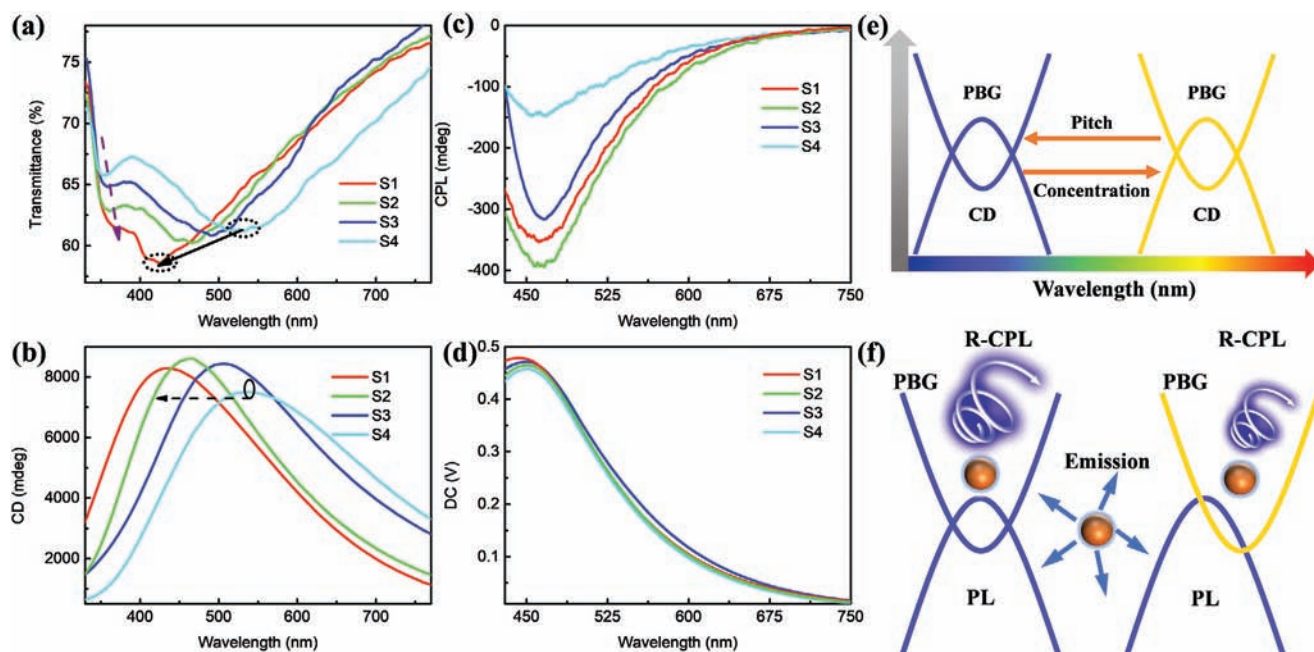


Figure 4. Chiral optical properties of the photonic films. a) Transmission and b) CD spectra of the photonic films. c) CPL spectra and d) DC curves of the photonic films. e) Illustration of the tunable CD of films that is regulated by the pitch of films. The left-handed helical structure of photonic films shows positive Cotton effect. The PBG could be easily tuned by varying the concentration of Si QDs due to different helical pitches. f) Schematic mechanism of the induced CPL which is the result of combination of PL and PBG.

the LD/LB could be eliminated by simple sample rotation and “front-back” measurement. As shown in Figure S5, Supporting Information, the recorded signals only show slight difference during the rotation and “front-back” measurements, which indicate the intrinsic nature of the CD signal. Figure 4b displays the CD spectrum of the photonic crystal films. It can be seen that all the films display a very strong and positive CD signal at the same position similar to the transmission spectrum. Similarly, the CD signal shows a blue shift from S4 to S1 with the increase of Si QDs concentration. In addition, CD measurements of the same concentration of Si QDs and CNC mixtures with various ultrasonic times are implemented (Figure S6, Supporting Information), which shows that the CD signal is closely related to the ultrasonic time. This can be ascribed to the different helical pitches formed after the EISA process due to different ultrasonic times.^[42,43] The CD signal of the chiral solid films might have several origins according to the length scales: a) molecular chirality from the D-glucose units of CNCs; b) chirality from Si QDs; c) morphology chirality of CNCs with screw shape; and d) chirality from the chiral nematic structure of CNCs self-assembly.^[43,44] Usually, the spectral position of the CD signal from biomolecules is shorter than 280 nm. Hence, the chirality of D-glucose unit in CNC could not be contributed to final signal of the solid film. Chirality measurements on the as-prepared Si QDs were performed as shown in Figure S6, Supporting Information. It can be seen that the Si QDs exhibit a very weak signal (only ≈ 1 mdeg) at 370 nm, which comes from the chirality transfer of glucose during synthesis. However, this induced chirality is too weak to contribute to the signal of the thin film. To confirm the origins, CD signal of the pure CNCs and mixtures of CNCs and

Si QDs with different concentrations are measured (Figure S7, Supporting Information). For both pure CNCs suspension and mixtures, no additional peak after adding Si QDs appears in both CD and absorption spectra, which indicates that the CD signal in the visible range could only come from the 1D PBG and the predominant left-handed helical structure. The transmission and CD spectra prove that all the films possess chiral photonic crystal structures with left handedness.^[29] In short, the as-prepared films have a left-handed helical structure which could selectively reflect left CPL and transmit right CPL. The selective reflection could be easily tuned by simply varying the concentration of Si QDs loading on CNCs which leads to different helical pitches (Figure 4e).

Apart from strong CD, CPL performance of all solid films is recorded under the excitation of 355 nm. The results are shown in Figure 4c,d. All the solid films show negative signal indicating that right CPL has been successfully achieved by the chiral photonic structures. It can be seen that sample S2 has the largest CPL while the signal of sample S4 is the weakest. g_{lum} is used to evaluate the degree of CPL, which is defined as:

$$g_{\text{lum}} = \frac{2(I_L - I_R)}{I_L + I_R} \quad (2)$$

where I_L and I_R are the intensity of left and right CPL, respectively. It could be seen that g_{lum} is ranging from 2 for ideal left CPL to -2 for ideal right CPL, where zero is corresponding to achiral emission. The value of g_{lum} for S2 is about -0.25 at 470 nm (Figure S8, Supporting Information), which is much bigger compared to other nanoparticles with induced CPL. For instance, ligand induced CPL from nanoparticles is usually on

the order of 10^{-3} to 10^{-5} .^[42,45,46] CPL measurement for the suspensions of corresponded solid films is conducted. There is no signal in the CPL spectrum of the suspensions. Therefore, it can be concluded that both the CPL and CD originate from the helical structure rather than the molecular chirality (Figure S9, Supporting Information). To understand the CPL behavior of different films, PBG of the films and emission from Si QDs are needed to be considered simultaneously. As shown in Figure 4f, the CPL signal is the strongest when the PBG coincides with the emission band of Si QDs, which results in the biggest dissymmetry factor. However, the signal shows a dramatic decrease when the PBG is far away from the emission band of Si QDs, which gives rise to a small dissymmetry factor.^[29]

The strong CPL response and outstanding dissymmetry factor of the films enables us to extend their application such as the enantioselective photopolymerization of diacetylene. It is known that the polydiacetylene (PDA) chain could display chiral order during the chain-propagating process with the introduction of CPL.^[47–49] Here, sample S2 is chosen to be the CPL source due to its largest dissymmetry factor and strongest CPL signal among all the films. The experimental setup is shown in Figure 5a. Typically, DA film is fabricated by a simple drop casting method. Sample S2 is excited by a 355 nm laser for generating R-CPL in the chiral film. Besides, a UV lamp with wavelength centered at 254 nm works simultaneously with induced R-CPL of S2. After exposing to the radiation for ≈ 20 min, the color of the DA film turns to blue which implies the formation of PDA. To confirm the interaction between the induced R-CPL and DA monomers, two contrast experiments (UV radiation only and CPL radiation only) are conducted and the experiment setups are shown in Figure S10, Supporting Information. Then, CD measurements are carried out for all the treated DA films. Typical results are displayed in Figure 5c. As mentioned previously, the recorded CD signal could also be generated from an order solid by linear dichroism (LD). To

eliminate the effect, LD measurement is carried out, and typical results are shown in Figure S11, Supporting Information. It can be seen that the LD contribution for the CD signal could be neglected. The CD spectrum (Figure 5c) exhibits that the obtained PDA film exposed synchronously under R-CPL and UV light shows a negative signal corresponding to the handedness of CPL while the other two obtained films display no signals in the spectrum. When the film is exposed to UV radiation, the absorption spectrum shows two distinct peaks at the same wavelength as the film exposed under the UV and CPL irradiation indicating the formation of PDA (Figure 5d). However, the film exposed to UV radiation is CD inactive proving that the film does not form a chiral order (Figure 5c). The film exposing only to CPL radiation display no signal in both the absorption and CD spectrum. The mechanism of enantioselective polymerization for DA films is shown in Figure 5e. According to previous reports, the wavelength of photo-initiation for polymerization reaction of DA should be shorter than 310 nm.^[50] Under UV irradiation, the DA monomer could form a dimer while the DA monomer exposed to CPL radiation could not be activated. After the formation of dimer, two strategies are considered feasible for the chain propagation process. The first method is that the energy is transferred from an excited monomer to the polymer chain in which the wavelength of light should be in the UV region. This process would compete with the photo initiation. The other strategy is to excite the polymer chain directly. It has been reported that the excitation energy would exhibit a dramatic decrease with increasing the chain length of PDA. The excitation wavelength could move to a visible range when the repeat units are more than 5. In this case, the induced CPL of photonic film could be used for exciting the oligomer chain directly. The interaction between the oligomer and induced CPL plays a vital role in the chain propagation process in which the chiral order is directly related to the handedness of CPL.

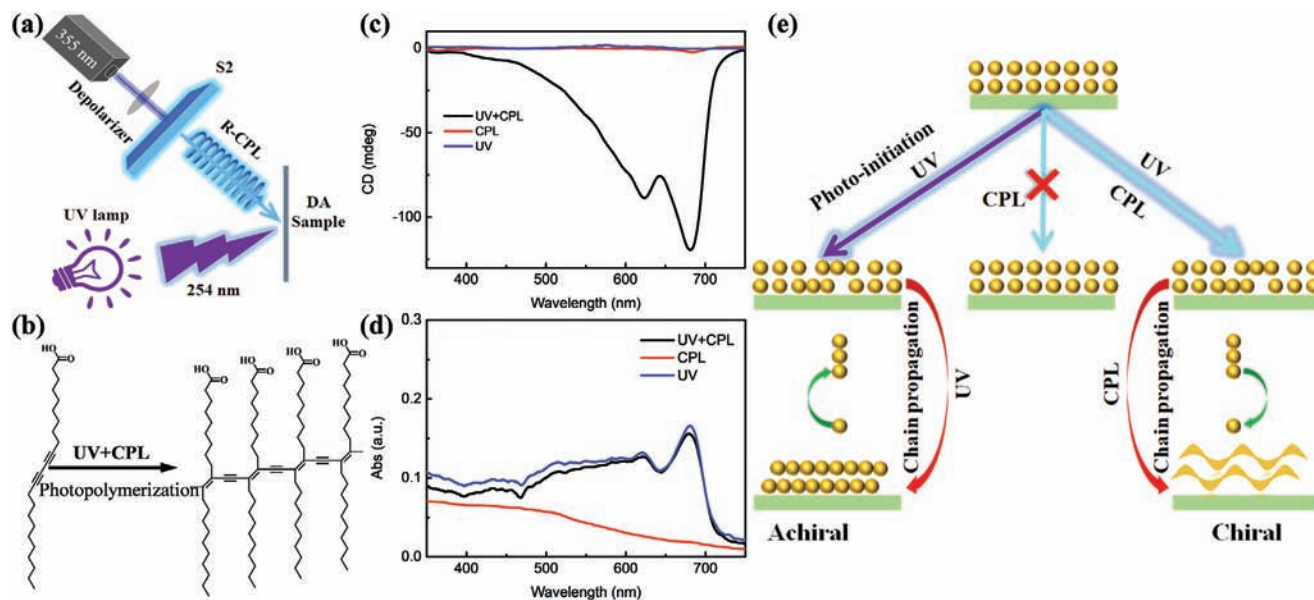


Figure 5. Photopolymerization of DA. a) Experimental setup for enantioselective photopolymerization of DA. b) Illustration of the polymerization. c) CD and d) UV spectra of films exposed to different light sources. e) Possible enantioselective photopolymerization mechanism for DA film.

3. Conclusion

In summary, Si QDs with excellent water solubility and stability are synthesized by a simple and environmental route. By incorporating Si QDs into CNCs template, solid Si QDs/CNCs composite films are obtained with 1D left-handed helical structure. The obtained composite films show tunable PBG and CD signal. Besides, CPL with a large dissymmetry factor is successfully achieved by the combination of emission from Si QDs and the chiral nematic structure of film. The dissymmetry factor could be manipulated by the PBG of the film. Enantioselective photopolymerization of DA with chiral order is realized by applying the CPL generated from the as-prepared photonic films working simultaneously with UV light. Our results disclose an easy and powerful platform based on earth abundant CNCs for the exploration of CPL-active nanomaterials with a high dissymmetry factor. This work also provides the proof-of-concept demonstration of the self-assembling hybrid nanoarchitecture as a chiral light source for enantioselective photopolymerization.

4. Experimental Section

Preparation of Si QDs: The Si QDs were prepared according to previous literature.^[33] Typically, 1 mL 3-APTES (99%, Sigma-Aldrich) was slowly added into 900 mg D-glucose (99.5%, Sigma-Aldrich) which was dissolved into 8 mL DI water under stirring. During the synthesis, the glucose was used as reductant. The solution needed to stir for 48 h at room temperature until the solution changed from colorless into brown color. After that, the solution was dialyzed for 6 h. Then, the obtained sample was stored in the refrigerator at 4 °C for further use.

Preparation of CNCs: CNC was prepared by a traditional sulfuric acid-catalyzed hydrolysis method that is widely reported.^[42] Typically, 10 g microcrystals cellulose from wood pulp was added to 100 g sulfuric acid (64 wt%) stirred at 45 °C in water bath for 90 min. The reaction was quenched by adding excess water. After that, the obtained suspension was washed with DI water by repeated centrifugation. Then, the precipitate was dialyzed using dialysis tubes with DI water until the PH value was constant. Finally, the obtained slurry was sonicated and stored in refrigerators at 4 °C for further use.

Preparation of CNCs-Si QDs Composite Film: Different volumes of Si QDs were added into the CNC suspensions (3 mL, 3.5 wt%). The final concentrations of Si QDs are summarized in Table S1, Supporting Information. Then, for obtaining homogenous solutions, the mixtures were sonicated for 15 min and stirred for 90 min at room temperature. After that, the suspensions were cast in a polystyrene petri with a diameter ≈35 mm and dried under ambient conditions for 2 days to obtain photonic films.

DA Films Fabrication for Photopolymerization: DA monomers were purchased from Aladdin. In short, DA was dissolved in DI water and ethanol mixture. Then, the mixture after ultrasonic treatment was directly dropped on the quartz substrate. After the monomer film was dried, the film was kept in a dark room for 12 h before photopolymerization.

Characterizations: TEM images were obtained using a HITACHI-HT7700 electron microscope. XPS was done using a PHI 5000Versaprobe III system of ULVAC-PHI. The FTIR spectroscopy was conducted on a BRUKER VERTEX 80 spectrometer. SEM was performed on a ZEISS-Merlin instrument with an accelerating voltage of 5 kV. POM images were obtained on a Nikon, Ci-POL polarized light microscope. The Zeta potential of CNC suspension and Si QDs solution were measured on a NanoBrook 90Plus Zeta. The UV-Vis spectrum (Figure 2d) of the Si QDs was obtained using PerkinElmer Lambda 750. The absorption spectrum shown in Figure S8, Supporting Information,

was collected by JASCO J-1500. Fluorescence spectra were measured on Edinburgh Instruments FLS1000 under excitation at 350 nm. The transmission of the photonic films was characterized by a UV-Vis-NIR microspectrophotometer (CRAIC technologies Inc.) where the photonic films were perpendicular to the incident beam during the measurement. CD spectra were obtained using a JASCO J-1500 CD spectrometer in which the scanning rate is 20 nm min⁻¹. CPL spectra were measured on a JASCO CPL-300.

Supporting Information

Supporting Information is available from the Wiley Online Library or from the author.

Acknowledgements

This work is supported by National Natural Science Foundation of China (62174079 and 22101118), Shenzhen Science and Technology Innovation Commission (Projects Nos. JCYJ20210324120204011 and KQTD2015071710313656) and National Natural Science Foundation of Hubei Province (No. 2020CFB200 and No. 2021CFB018).

Conflict of Interest

The authors declare no conflict of interest.

Data Availability Statement

The data that support the findings of this study are available from the corresponding author upon reasonable request.

Keywords

cellulose nanocrystals, circularly polarized luminescence, photopolymerization, quantum dots, self-assembly

Received: April 2, 2022
Published online: May 28, 2022

- [1] I. C. Seo, Y. Lim, S.-C. An, B. H. Woo, S. Kim, J. G. Son, S. Yoo, Q. H. Park, J. Y. Kim, Y. C. Jun, *ACS Nano* **2021**, *15*, 13781.
- [2] C. He, Z. Feng, S. Shan, M. Wang, X. Chen, G. Zou, *Nat. Commun.* **2020**, *11*, 1188.
- [3] D. Han, X. Yang, J. Han, J. Zhou, T. Jiao, P. Duan, *Nat. Commun.* **2020**, *11*, 5659.
- [4] J. Chen, J. Hu, H. Yu, *ACS Nano* **2021**, *15*, 4372.
- [5] H. Lu, J. Wang, C. Xiao, X. Pan, X. Chen, R. Brunecky, J. J. Berry, K. Zhu, M. C. Beard, Z. V. Vardeny, *Sci. Adv.* **2019**, *5*, eaay0571.
- [6] G. Long, R. Sabatini, M. I. Saidaminov, G. Lakhwani, A. Rasmita, X. Liu, E. H. Sargent, W. Gao, *Nat. Rev. Mater.* **2020**, *5*, 423.
- [7] K. Trujillo-Hernández, G. Rodríguez-López, A. Espinosa-Roa, J. González-Roque, A. P. Gómora-Figueroa, W. Zhang, P. S. Halasyamani, V. Jancik, M. Gembicky, G. Pirruccio, D. Solis-Ibarra, *J. Mater. Chem. C* **2020**, *8*, 9602.
- [8] Y.-H. Kim, Y. Zhai, H. Lu, X. Pan, C. Xiao, E. A. Gaubing, S. P. Harvey, J. J. Berry, Z. V. Vardeny, J. M. Luther, M. C. Beard, *Science* **2021**, *371*, 1129.

- [9] J.-X. Gao, W.-Y. Zhang, Z.-G. Wu, Y.-X. Zheng, D.-W. Fu, *J. Am. Chem. Soc.* **2020**, *142*, 4756.
- [10] Y. Hu, F. Florio, Z. Z. Chen, W. A. Phelan, M. A. Siegler, Z. Zhou, Y. W. Guo, R. Hawks, J. Jiang, J. Feng, L. F. Zhang, B. W. Wang, Y. P. Wang, D. Gall, E. F. Palermo, Z. H. Lu, X. Sun, T.-M. Lu, H. Zhou, Y. Ren, E. Wertz, R. Sundararaman, J. Shi, *Sci. Adv.* **2020**, *6*, eaay4213.
- [11] C. Zhang, S. Li, X.-Y. Dong, S.-Q. Zang, *Aggregate* **2021**, *2*, e48.
- [12] J. Hao, F. Zhao, Q. Wang, J. Lin, P. Chen, J. Li, D. Zhang, M. Chen, P. Liu, M.-H. Delville, T. He, J. Cheng, Y. Li, *Adv. Opt. Mater.* **2021**, *9*, 2101142.
- [13] J. Hao, Y. Li, J. Miao, R. Liu, J. Li, H. Liu, Q. Wang, H. Liu, M.-H. Delville, T. He, K. Wang, X. Zhu, J. Cheng, *ACS Nano* **2020**, *14*, 10346.
- [14] J. Cheng, J. Hao, H. Liu, J. Li, J. Li, X. Zhu, X. Lin, K. Wang, T. He, *ACS Nano* **2018**, *12*, 5341.
- [15] M. Naito, K. Iwahori, A. Miura, M. Yamane, I. Yamashita, *Angew. Chem., Int. Ed.* **2010**, *49*, 7006.
- [16] U. Tohgha, K. K. Deol, A. G. Porter, S. G. Bartko, J. K. Choi, B. M. Leonard, K. Varga, J. Kubelka, G. Muller, M. Balaz, *ACS Nano* **2013**, *7*, 11094.
- [17] Y. Han, Y. Chen, J. Feng, J. Liu, S. Ma, X. Chen, *Anal. Chem.* **2017**, *89*, 3001.
- [18] A. N. Thiessen, L. Zhang, A. O. Oliynyk, H. Yu, K. M. O'Connor, A. Meldrum, J. G. C. Veinot, *Chem. Mater.* **2020**, *32*, 6838.
- [19] J. Liang, Y. Wu, X. Gong, A. Vomiero, *J. Mater. Chem. C* **2021**, *9*, 1746.
- [20] J. G. C. Veinot, *Chem. Commun.* **2006**, 4160.
- [21] L. Mangolini, U. Kortshagen, *Adv. Mater.* **2007**, *19*, 2513.
- [22] R. K. Baldwin, K. A. Pettigrew, E. Ratai, M. P. Augustine, S. M. Kauzlarich, *Chem. Commun.* **2002**, 1822.
- [23] Q. Wen, C. Pan, X. Qin, Q. Ma, S. Feng, *Anal. Methods* **2021**, *13*, 390.
- [24] B. Sharma, S. Tanwar, T. Sen, *ACS Sustainable Chem. Eng.* **2019**, *7*, 3309.
- [25] S. T. Selvan, P. K. Patra, C. Y. Ang, J. Y. Ying, *Angew. Chem., Int. Ed.* **2007**, *46*, 2448.
- [26] M. Xu, C. Ma, J. Zhou, Y. Liu, X. Wu, S. Luo, W. Li, H. Yu, Y. Wang, Z. Chen, J. Li, S. Liu, *J. Mater. Chem. C* **2019**, *7*, 13794.
- [27] X. M. Dong, D. G. Gray, *Langmuir* **1997**, *13*, 2404.
- [28] Y. Habibi, L. A. Lucia, O. J. Rojas, *Chem. Rev.* **2010**, *110*, 3479.
- [29] H. Zheng, B. Ju, X. Wang, W. Wang, M. Li, Z. Tang, S. X.-A. Zhang, Y. Xu, *Adv. Opt. Mater.* **2018**, *6*, 1801246.
- [30] I. Ortiz-Gómez, V. Toral-López, F. J. Romero, I. de Orbe-Payá, A. García, N. Rodríguez, L. F. Capitán-Vallvey, D. P. Morales, A. Salinas-Castillo, *Sens. Actuators, B* **2021**, *332*, 129506.
- [31] X. M. Dong, T. Kimura, J.-F. Revol, D. G. Gray, *Langmuir* **1996**, *12*, 2076.
- [32] Y. Han, W. Lv, H. Chen, H. Li, J. Chen, Z. Li, H. Qiu, *Anal. Chem.* **2020**, *92*, 3949.
- [33] J. Wu, J. Dai, Y. Shao, Y. Sun, *RSC Adv.* **2015**, *5*, 83581.
- [34] H. Liu, Y. He, J. Mu, K. Cao, *Spectrochim. Acta, Part A* **2022**, *266*, 120421.
- [35] X. Cheng, S. B. Lowe, P. J. Reece, J. J. Gooding, *Chem. Soc. Rev.* **2014**, *43*, 2680.
- [36] K. Hola, A. B. Bourlinos, O. Kozak, K. Berka, K. M. Siskova, M. Havrdova, J. Tucek, K. Safarova, M. Otyepka, E. P. Giannelis, R. Zboril, *Carbon* **2014**, *70*, 279.
- [37] S. H. Jin, D. H. Kim, G. H. Jun, S. H. Hong, S. Jeon, *ACS Nano* **2013**, *7*, 1239.
- [38] E. V. Shevchenko, M. I. Bodnarchuk, M. V. Kovalenko, D. V. Talapin, R. K. Smith, S. Aloni, W. Heiss, A. P. Alivisatos, *Adv. Mater.* **2008**, *20*, 4323.
- [39] W. Li, M. Xu, C. Ma, Y. Liu, J. Zhou, Z. Chen, Y. Wang, H. Yu, J. Li, S. Liu, *ACS Appl. Mater. Interfaces* **2019**, *11*, 23512.
- [40] L. Xu, J. Xu, W. Li, Z. Weiming, P. Sun, Z. Ma, X. Huang, K. Chen, *J. Mater. Sci.* **2007**, *42*, 9696.
- [41] G. Albano, G. Pescitelli, L. Di Bari, *Chem. Rev.* **2020**, *120*, 10145.
- [42] Y. Shi, Z. Zhou, X. Miao, Y. J. Liu, Q. Fan, K. Wang, D. Luo, X. W. Sun, *J. Mater. Chem. C* **2020**, *8*, 1048.
- [43] G. Chu, X. Wang, T. Chen, W. Xu, Y. Wang, H. Song, Y. Xu, *J. Mater. Chem. C* **2015**, *3*, 3384.
- [44] H. Qi, K. E. Shopsowitz, W. Y. Hamad, M. J. MacLachlan, *J. Am. Chem. Soc.* **2011**, *133*, 3728.
- [45] M. V. Mukhina, V. G. Maslov, A. V. Baranov, A. V. Fedorov, A. O. Orlova, F. Purcell-Milton, J. Govan, Y. K. Gun'ko, *Nano Lett.* **2015**, *15*, 2844.
- [46] Y. Zhou, R. L. Marson, G. van Anders, J. Zhu, G. Ma, P. Ercius, K. Sun, B. Yeom, S. C. Glotzer, N. A. Kotov, *ACS Nano* **2016**, *10*, 3248.
- [47] G. Yang, L. Zhu, J. Hu, H. Xia, D. Qiu, Q. Zhang, D. Zhang, G. Zou, *Chem. - Eur. J.* **2017**, *23*, 8032.
- [48] Y. Xu, G. Yang, H. Xia, G. Zou, Q. Zhang, J. Gao, *Nat. Commun.* **2014**, *5*, 5050.
- [49] X. Jin, Y. Sang, Y. Shi, Y. Li, X. Zhu, P. Duan, M. Liu, *ACS Nano* **2019**, *13*, 2804.
- [50] G. Yang, L. Han, H. Jiang, G. Zou, Q. Zhang, D. Zhang, P. Wang, H. Ming, *Chem. Commun.* **2014**, *50*, 2338.